TITLE: Transonic Buffet of a Supercritical
Airfoil

TITLE: Verification and Validation Data for
Computational Unsteady Aerodynamics [Donnees de
verification et de valadation pour
l'aerodynamique instationnaire numerique]

13E TRANSONIC BUFFET OF A SUPERCRITICAL AIRFOIL

Reported by
X.Z. Huang
of work by
B.H.K. Lee and F.C. Tang, et al

INTRODUCTION

This investigation was carried out in the Institute for Aerospace Research (IAR) 2D High Reynolds Test Facility (Ref. 1 to Ref. 3 and Fig. 1) to study the buffet characteristics of a supercritical airfoil, BGK No. 1 (Fig. 2). Steady, unsteady surface pressure and normal force were measured at various angles of attack and Mach numbers. The statistical properties of the normal force and pressure were carried out by spectral analyses. Buffet onset boundaries were evaluated from the divergence of the fluctuating normal force while buffet intensities were determined from the normal force measurements. The attached and separated flow regions on the airfoil as well as the merging of a shock induced separation bubble with the trailing edge separation region were determined by skin friction measurements.

The test program is presented in Table 1. There are two BGK No.1 models. One has normal static pressure orifices and 6 pressure ports to measure pressure fluctuations (BGK-1). Another has 15 fast response transducers (BGK-1(m)). The model's coordinates and the locations of pressure orifices and transducers are listed in Table 2 Table 3 respectively (in CD ROM). The experimental arrangement and results have been described in detail in Ref. 4 to Ref. 9. Tabulated data and illustrations are presented in Table 4 to Table 7 and Fig. 3 to Fig. 16 in CD ROM with part of the illustrations shown here.

Fig. 3 and Table 4 show the fluctuating normal force on BGK–1 model for various Mach numbers. Typical power spectra of the normal force are shown in Fig. 4. The frequencies of the shock motion vary from 70-80 Hz for the Mach number range of 0.688~0.796 and are partly listed in Table 5. The flow conditions where discrete shock oscillations were detected are summarized in Fig. 5. The test program for BGK-1(m) in Table 1 can be sorted in three cases as seen in Fig. 5: 1) points A, B, C, D, and E; 2) points a, b, c, d and e; and 3) points 1, 2, 3, 4, and 5 respectively. The shaded region was obtained by fixing a Mach number but varying the incidence in the experiment. A power spectra plot of the normal force was computed at each α and the presence of shock waves was determined from observing whether the 70-80 Hz peak was present or not. The buffet boundary, which was obtained from divergence of the fluctuating normal force, is included in this figure for reference. This buffet onset is identified from the divergence of the normal force fluctuations by noting the point on the curve with a slope $dC_N/dC_L=0.1$. This value is arbitrarily chosen, but in those cases where buffet onset is primarily due to trailing edge separations, this criterion for deriving the buffet boundary is found to give consistent results and agrees with values computed from trailing edge pressure divergence.

The static surface pressure distributions are listed in Table 6 with some examples shown here from Fig. 6 to Fig. 8. The cross-hatched and open bar symbols in Fig. 7 and Fig. 8 denote regions of attached and separated flows determined from skin friction measurements.

Table 7 presents the unsteady pressure or the pressure intensities along airfoil chord of BGK-1 and BGK-1(m) models. The corresponding figures are shown in Fig. 10 and Fig. 11.

The statistical properties such as power and cross power spectral density, auto and cross correlation functions, as well as coherence functions of pressure and normal force have been measured at different Mach numbers and angles of attack. As examples Fig. 12 shows a set of the spectral analyses at the condition of M=0.753 and α=5.66° for BGK-1 model. The frequency response of the installed transducers was calibrated and established to be flat up to approximately 200 Hz. The normal force signal was obtained at the sampling frequency of 1.6 kHz. Power spectra of unsteady pressure on upper surface of BGK-1(m) at different locations are shown from Fig. 13a to Fig. 13c. Fig. 14 shows the cross correlation functions between different transducers at M=0.688 and α=3.99°, 6.43° and 9°.

The pressure-time histories on BGK-1(m) model at M=0.71 and various α are presented in Fig. 15. The unsteady pressure fluctuations behind the periodic shock wave have two contributions. One is from a random component associated with the turbulent motion in the separated flow region. Another is a deterministic part from the pressure field as a result of shock wave oscillation. Thus, approximately 175 ensemble averages of the pressure signals were performed. Each ensemble, which was synchronized to the zero crossings decided from balance normal force spectra, had 32 samples. A Fourier analysis was then performed to obtain the fundamental and harmonics of the oscillatory pressure field.

For supercritical airfoils such as the BGK No. 1, it is found that at the lower Mach number range, separation can occur behind the shock wave as a bubble and propagates downstream as the angle of incidence is increased. Trailing edge separation can occur at the same time and it moves upstream and the two separated regions will eventually merge. An investigation on the model was carried out at M=0.688 using a Preston tube to measure the skin friction on the surface at various angles of attack. The typical distributions of the skin friction coefficient are presented in Fig. 16. The results show that at α=4.67°, a small separation bubble begins to form behind the shock wave. The separation bubble grows as the incidence increased and at α=6.15°, trailing edge separation has already begun and has moved to nearly 90% of the chord as seen in Fig. 16.

LIST OF SYMBOLS AND DEFINITIONS

b	model span	
c	model chord	
C_L	lift coefficient	$=\frac{L}{qbc}$
C_{Ldes}	design lift coefficient	
C_N	normal force coefficient	$=\frac{N}{qbc}$
C_p	pressure coefficient	$=\frac{p-p_\infty}{q}$
$\overline{C}_p$	ensemble-averaged pressure coefficient	
$C_p^{'}$	fluctuating pressure coefficient	$=\frac{P_{rms}}{q}$
$C_N^{'}$	fluctuating normal force coefficient	$=\frac{N_{rms}}{qbc}$
f	frequency	
L	lift	
M	free stream Mach number	
M_{des}	design Mach number	
M_{dr}	drag rise Mach number	
N	Normal force	
$\overline{N}$	time-averaged normal force	
N_{rms}	rms value of normal force	$Nrms=\sqrt{\lim_{T\to\infty}\frac{1}{T}\int_0^T(N-\overline{N})^2(t)dt}$
P	local static pressure	
P_∞	free stream static pressure	
$\overline{P}$	time-averaged pressure	
P_{rms}	rms value of the fluctuating pressure	$P_{rms}=\sqrt{\lim_{T\to\infty}\frac{1}{T}\int_0^T(P-\overline{P})^2(t)dt}$
Q,q	free stream dynamic pressure	

Re	Reynolds number based on chord	
$R_x(\tau)$	auto correlation function of x(t)	$R_x(\tau) = \lim_{T\to\infty} \frac{1}{T} \int_0^T x(t) \cdot x(t+\tau) dt$
$R_{xy}(t)$	cross correlation function of x(t) and y(t)	$R_{xy}(\tau) = \lim_{T\to\infty} \frac{1}{T} \int_0^T x(t) \cdot y(t+\tau) dt$
$S_x(f)$	power spectral density of x(t)	$S_x(f) = 2 \int_{-\infty}^{\infty} R_x(\tau) e^{-i2\pi f\tau} d\tau$
Sxy(f)	cross power spectral density of x(t) and y(t)	$S_{xy}(f) = 2 \int_{-\infty}^{\infty} R_{xy}(\tau) e^{-i2\pi f\tau} d\tau$
t,T	time	
x	distance measured along chord from the leading edge	
x(t)	random signal	
y(t)	random signal	
α	mean wing incidence	
γ_{xy}^2	coherence function of x(t) and y(t)	$\gamma_{xy}^2 = \frac{\lvert S_{xy(f)} \rvert^2}{S_x(f) \cdot S_y(f)}$
τ	time delay	

FORMULARY

1 General Description of model

1.1	Designation	Bauer-Garabedian-Korn (BGK No. 1) airfoil
1.2	Type	Aft-loaded, natural laminar flow-capable, shock-free supercritical airfoil
1.3	Design condition	Potential flow M_{des}=0.72, M_{dr}=0.75, C_{Ldes}=0.63
1.4	Additional remarks	
1.5	References	Ref. 10

2 Model Geometry

2.1	Chord length	10 in
2.2	Span	15 in
2.3	Model coordinate	See Table 2 in CD ROM
2.4	Nose radius	-
2.5	Maximum thickness	t/c = 11.8%
2.6	Trailing edge thickness	0.1% of the chord
2.7	Additional remarks	
2.8	References	Ref. 4, 10

3 Wind Tunnel

3.1	Designation	IAR 2D High Reynolds Test Facility
3.2	Type of tunnel	Blowdown, closed test section
3.3	Test section dimensions	Rectangular, height 60 in, width 15 in, (see Fig. 1a)

3.4	Length of parallel section	141 in.
3.5	Floor and ceiling porosity	20.5%
3.6	Side wall boundary layer	A gap between inlet and nozzle section permit bleeding into the plenum chamber of fairly thick side wall boundary layer (~2 in.), see Fig. 1b.
3.7	Side wall near model area	Additional porous with boundary layer suction to atmospheric, see Fig. 1c.
3.8	Ventilation geometry	See Fig. 1d.
3.9	Range of Mach numbers	0.1 to 1.1
3.10	Re	$40x10^6$/ft at M=1, 10 seconds total run time
3.11	Wake traverse probe	7 wafer (12 ports) Statham miniature transducer unit
3.12	Turbulence intensity level	0.1% for Re/ft $\leq 6x10^6$
		0.16~0.24% for Re/ft $10x10^6$~$27x10^6$
3.13	Turbulence intensity level	0.1% for Re/ft $\leq 6x10^6$
		0.16~0.24% for Re/ft $10x10^6$~$27x10^6$
3.14	Reference on tunnel	Ref. 1, 2 and 3

4 Measurements and Observations

4.1	Steady pressure for the mean conditions	measured directly
4.2	Unsteady pressure for the mean conditions	measured directly
4.3	Steady forces for the mean conditions	measured directly
4.4	Unsteady forces for the mean conditions	measured directly
4.5	Spectral analysis of the pressure	yes
4.6	Spectral analysis of the loads	yes
4.7	Local skin friction	yes
4.8	Buffet boundaries	yes
4.9	Synchronous Cp time histories	yes

5 Test Conditions

5.1	Tunnel height/model chord ratio	6
5.2	Tunnel width/model chord ratio	1.5
5.3	Range of Mach number	0.501 ~ 0.805
5.4	Incidence range	-0.36 ~ 11.74
5.5	Reynolds number range	$15x10^6$ ~$20x10^6$
5.6	Range of tunnel total pressure	300 psi
5.7	Maximum mass flow	10 lbm/sec
5.8	Definition of model incidence	between "x" of model axis (Fig. 2) and tunnel axis
5.9	Position of transition, if free	Not applicable
5.10	Flow instabilities during tests	No evidence
5.11	Model deformation under the loads	Negligible
5.12	References describing tests	Ref. 4 to Ref. 9

6 Instrumentation

6.1	Steady pressure measurements for BGK-	

1 model	
6.1.1 Position of orifices	See Fig. 2a and Table 3 in CD ROM
6.1.2 Type of measuring system	70 pressure tubes + 15 in situ pressure transducers
6.2 Unsteady pressure measurements for BGK-1 model	
6.2.1 Location of transducers	See Fig. 2a (in the middle chord) and Table 3 in CD ROM
6.2.2 Type of transducers	6 Kulite TQ 360 25 psid transducers
6.2.3 Dynamic response	Flat up to approximately 200 Hz.
6.2.4 Signal record	Recorded on FM tape for subsequent analysis.
6.2.5 Data reduction	
6.3 Unsteady pressure measurement for model BGK-1(m) model	
6.3.1 Location of transducers	See Fig. 2b and Table 3 in CD ROM
6.3.2 Type of transducers	16 of 25 psid custom made CQ-062-25D differential Kulite transducers
6.3.3 Diameter of screen	0.042 in.
6.3.4 Type of screen	0.005 in thick with 0.062 in diameter holes in a mesh pattern
6.3.5 Signal measurements	Signals were filtered by a four pole low pass filter having a 300 Hz 3db point and a –24 db/octave slope beyond 600 Hz.
6.3.6 Sampling rate	1.6 kHz
6.4 Loads measurement	
6.4.1 Type of sensors	strain gages
6.4.2 Balance	3 component side balance with max capacity of N=20,000 lbf, m=22,500 in.lb and X=2,000 lbf
6.4.3 Pitch drive system	Range: 55° maximum angular rate: 12° /sec, fully loaded step program: 0.25°, 0.5°, 1°, 2°, 5° ramp program: 0° – 10°/sec
6.4.4 Sampling rate	1.6 kHz
6.5 Skin friction measurement	
6.5.1 Type of transducers	Given by the difference between the total and static pressures
6.5.2 Method of measurement	Preston tube to determine the pitot pressure
6.5.3 Spatial resolution	0.05c for x > 0.6c and 0.02c for x < 0.6c respectively

7 Data presentation

7.1 Test cases	See Table 1
7.2 Normal force fluctuation	Fig. 3, Fig. 4 and Table 4 in CD ROM
7.3 Shock oscillation frequencies	Table 5 in CD ROM
7.4 Region of shock oscillation	Fig. 5
7.5 Steady pressure	Fig. 6 to Fig. 9 and Table 6 in CD ROM
7.6 Unsteady pressure	Fig. 10, Fig. 11 and Table 7 in CD ROM
7.7 Spectral analysis	Fig. 12, Fig. 13 and Fig. 14
7.7.1 Power spectral density	Fig. 12a and Fig. 13

7.7.2	Auto correlation functions	Fig. 12b
7.7.3	Cross correlation functions	Fig. 12c and Fig. 14
7.7.4	Cross power spectral density	Fig. 12d
7.7.5	Coherence function	Fig. 12e
7.7.6	Cross power spectral density and coherence function between pressure and normal force	Fig. 12f
7.7.7	Pressure-time histories	Fig. 15
7.8	Skin friction	Fig. 16
7.9	Example illustrations of results	Fig. 6, Fig. 7, Fig. 8, Fig. 10 to Fig. 16

8 Comments on data

8.1	Mach number	Mach number be maintained constant by control system
8.2	Steady incidence	measured by a potentiometer
8.3	Balance linearity	maximum 0.3% and generally < 0.1%
8.4	Balance interaction	<1.26%
8.5	Balance natural frequencies	140, 215, 320, 360 Hz, buffet excitation frequencies=70-80 Hz
8.6	Unsteady pressure coefficients	a discrete frequency of ≈420 Hz was detected due to tunnel disturbances (See Fig. 4)
8.7	Wall interference corrections	distributed suction was applied through porous plates in the vicinity of the model to minimize any three-dimensional effects

9 Personal contact for further information

X.Z. Huang, Aerodynamics Laboratory, Institute for Aerospace Research, National Research Council of Canada
M-10, IAR/NRC, Montreal Rd. Ottawa, Ontario, Canada, K1A 0R6
e-mail: xingzhong.huang@nrc.ca

10 List of references

[1] Ohman, L.H., "The NAE High Reynolds Number 15" x 60" Two-Dimensional Test Facility", National Research Council, NAE LTR-HA-4, Part 1, April 1970.

[2] Khalid, M., Ellis, F. and Ohman, H., "Flow Quality Measurements in the NAE 2D High Reynolds Number Trisonic Test Facility," NAE HAS-384, 1988.

[3] Chan, Y.Y., Tang, F.C. and Wolfe, S.M., "Analysis of the Boundary Layer Development on the Sidewalls of the NAE 2-D Test Facility," NAE LTR-HA-34, 1978.

[4] Lee, B.H.K. and Ohman, L.H., "Unsteady Pressure and Force Measurements Associated with Transonic Buffeting of a Two-Dimensional Supercritical Airfoil", National Research Council of Canada, AN-14, June 1983.

[5] Lee, B.H.K. and Ohman, L.H., "Unsteady Pressures and Forces During Transonic Buffeting of a Supercritical Airfoil", Journal of Aircraft, Vol. 21, No. 6, June 1986, pp. 439-441.

[6] Lee, B.H.K., Tang, F.C., Ellis, F.A. and Bureau, J., "Measurements of Buffet Characteristics of Supercritical Airfoils", 69th Semi-Annual Meeting of the Supersonic Tunnel Association, Manhattan Beach, California, May 1988.

[7] Lee, B.H.K., "Investigation of Flow Separation on a Supercritical Airfoil", Journal of Aircraft, Vol. 26, November 1989, pp. 1032-1037.

[8] Lee, B.H.K., "Transonic Buffet on a Supercritical Aerofoil", Aeronautical Journal, Vol. 94, No. 935, May 1990, pp. 143-152.

[9] Lee, B.H.K., "Flow Separation on a Supercritical Airfoil", Canadian Aeronautics and Space Institute Journal, Vol. 36, No. 2, June 1990, pp. 81-89.

[10] Kacprzynski, J.J., "An Experimental Analysis and Buffet investigation of the Shockless Lifting Airfoil No.1," NRC/NAE LR-569, Aug. 1973.

[11] Redeker, G. and Proksch, H.J., "The Prediction of Buffet Onset and Light Buffet by Means of Computational Methods," AGARD CP-204, 1977.

Table 1 Test matrix

M_∞	$Re_c x10^{-6}$	α°	C_L	Model	Cases in Fig. 5
0.501	21.0	11.74	1.124	BGK-1	
0.703	21.3	-0.31, 6.77,8.71	0.278, 1.077, 1.02	BGK-1	
0.753	21.1	5.66	0.945	BGK-1	
0.775	15.3	2.55, 3.57, 4.61	0.762,0.859, 0.868	BGK-1	
0.783	21.0	-0.34, 2.55, 3.55, 4.57, 5.60, 6.61	0.304, 0.756, 0.807, 0.820, 0.827, 0.84	BGK-1	
0.805	20.9	-0.36,3.52	0.314,0.727	BGK-1	
0.597	20.0	5.95		BGK-1(m)	a
0.688	20.0	3.99, 4.95, 6.43, 6.94, 9.0	0.981, 1.052, 1.059, 1.052, 1.069	BGK-1(m)	A,B,C,D,E
0.688	20.0	3.99, 4.45, 4.67, 4.95, 5.16, 5.44		BGK-1(m)	
		5.65, 5.92, 6.15, 6.43, 6.67		skin friction	b
0.71	20.0	-0.316, 1.396, 3.017, 4.905, 6.97	0.322, 0.610, 0.886, 1.034, 1.016	BGK-1(m)	1,2,3,4,5
0.722	20.0	5.98		BGK-1(m)	c
0.747	20.0	6.01	0.916	BGK-1(m)	d
0.772	20.0	6.04		BGK-1(m)	e

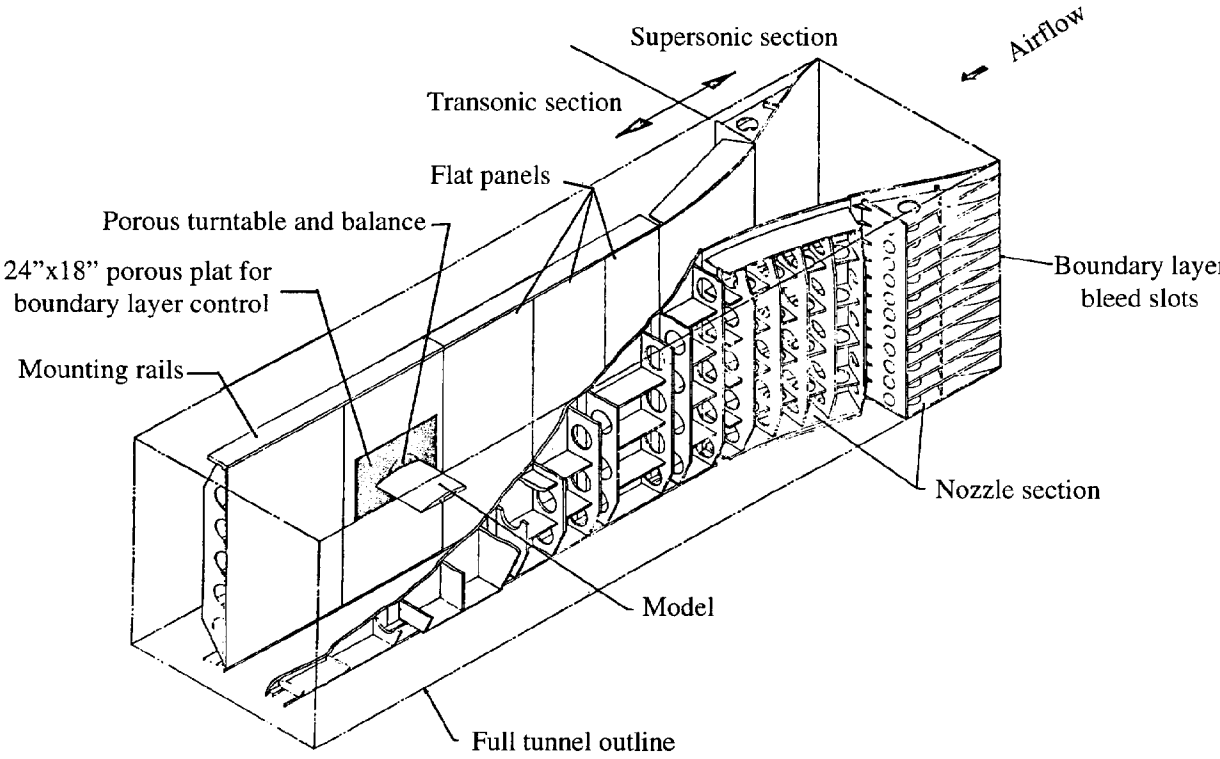

Fig. 1a IAR 15 in x 60 in 2-D insert

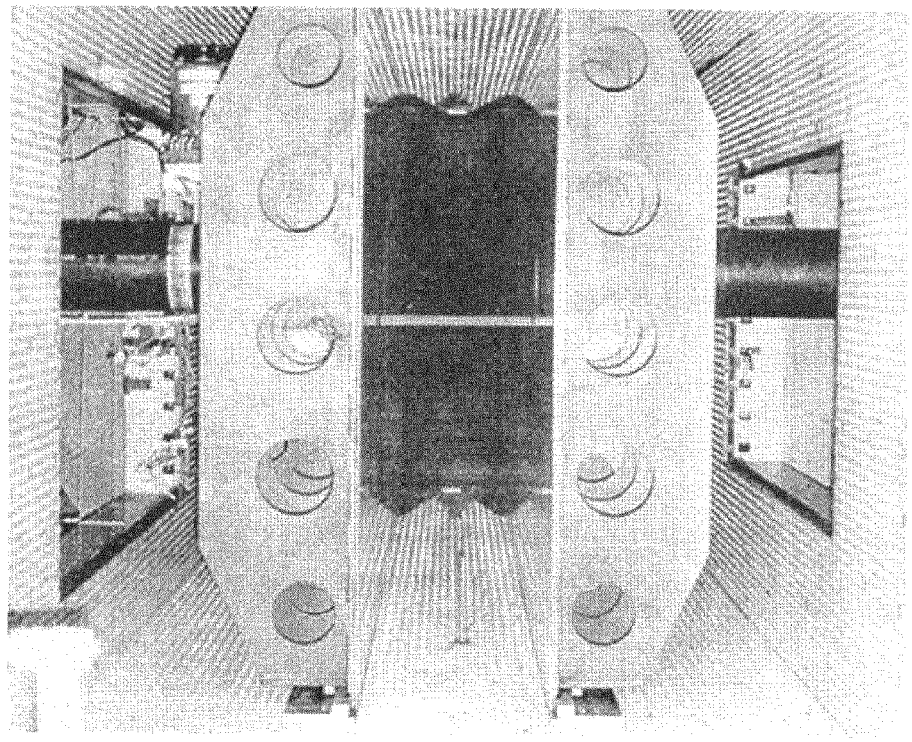

Fig. 1b Downstream view of 2-D insert

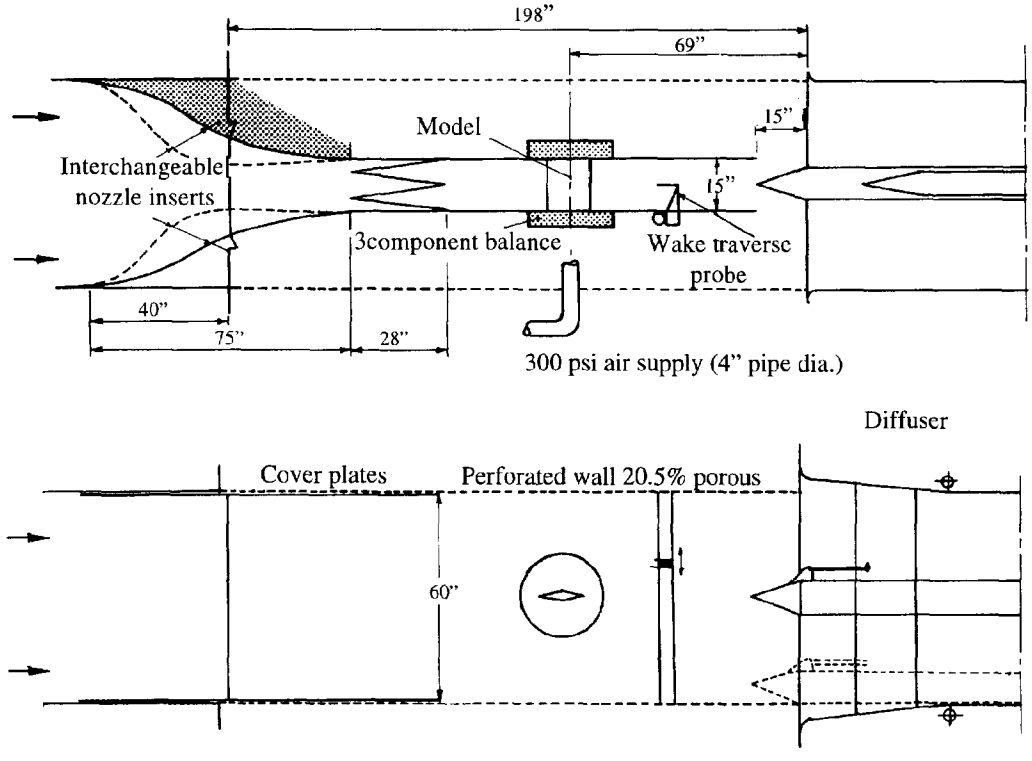

Fig. 1c 2D section arrangement for IAR 5ft x5ft wind tunnel

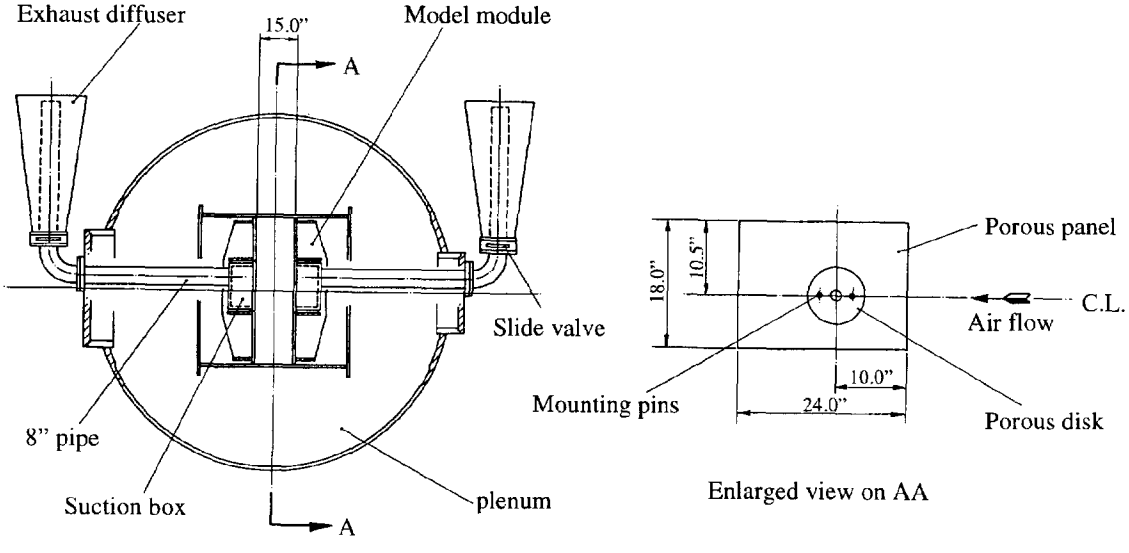

Fig. 1d Suction arrangement

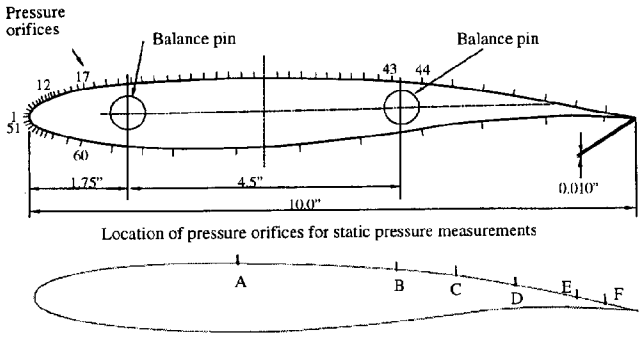

2a BGK-1 model

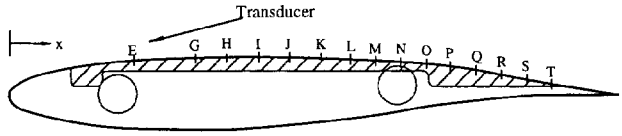

2b BGK-1(m) model

Fig. 2 BGK No. 1 supercritical airfoil

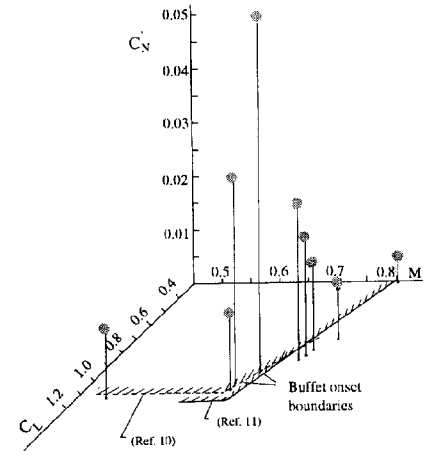

Fig. 3 Variation of the fluctuating normal force coefficient with Mach number and steady state lift coefficient

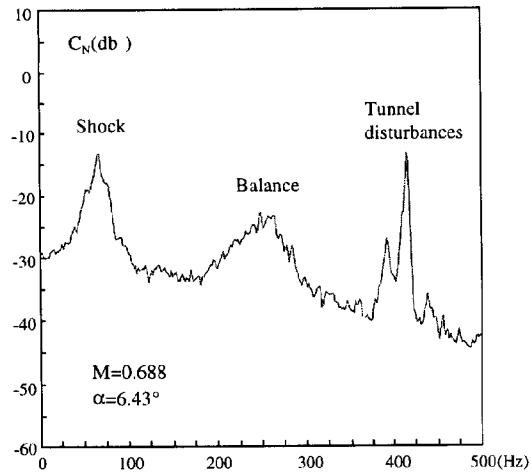

Fig. 4 Power spectra of normal force

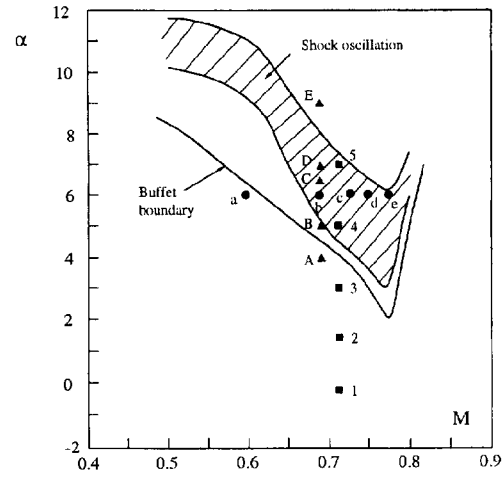

Fig. 5 Region of shock oscillation

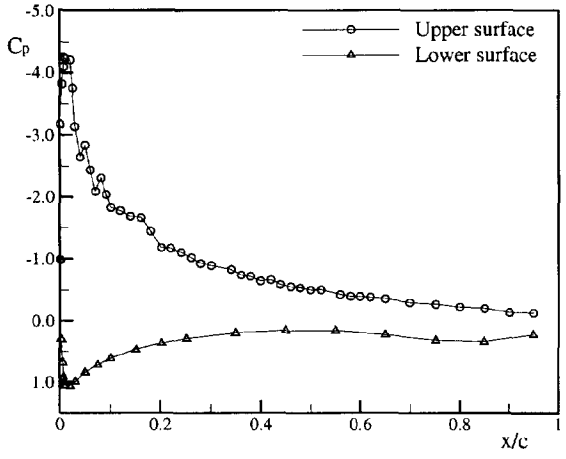

6a M=0.501, α=11.8°

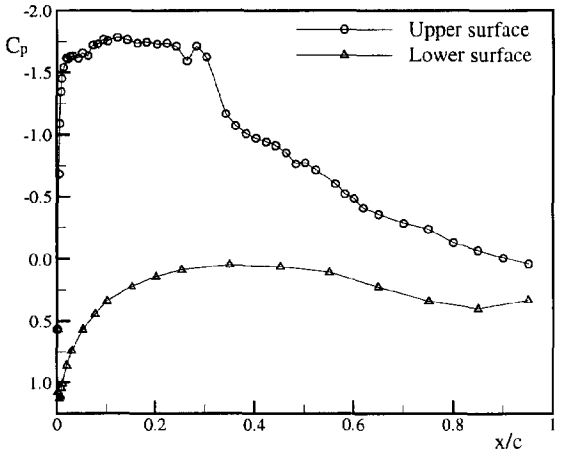

6b M=0.704, α=6.79°

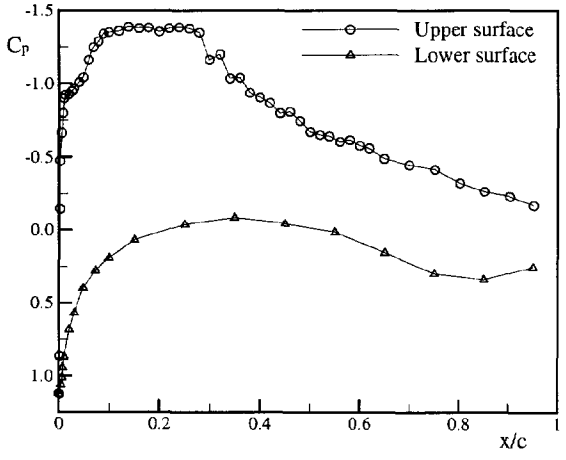

6c M=0.757, α=5.57°

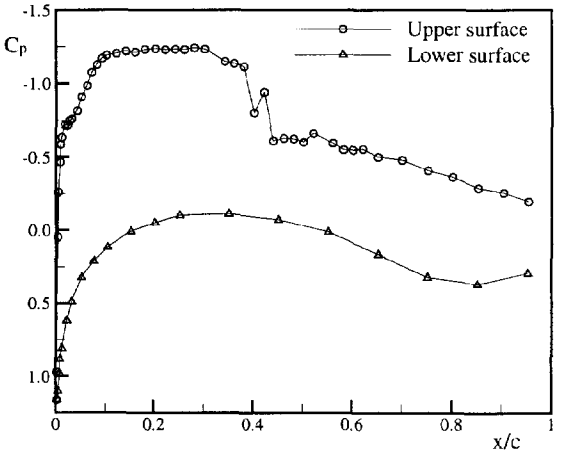

6d M=0.773, α=4.60°

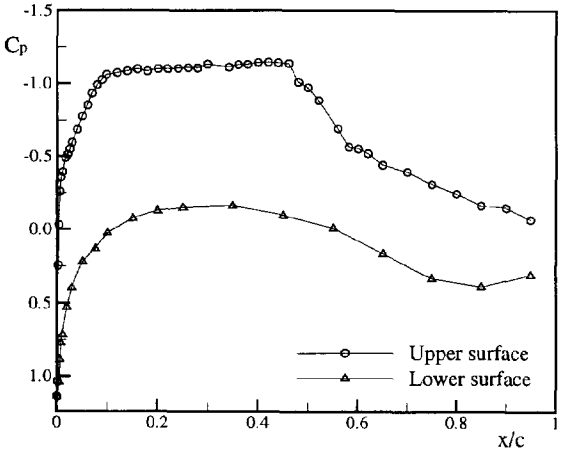

6e M=0.784, α=3.58°

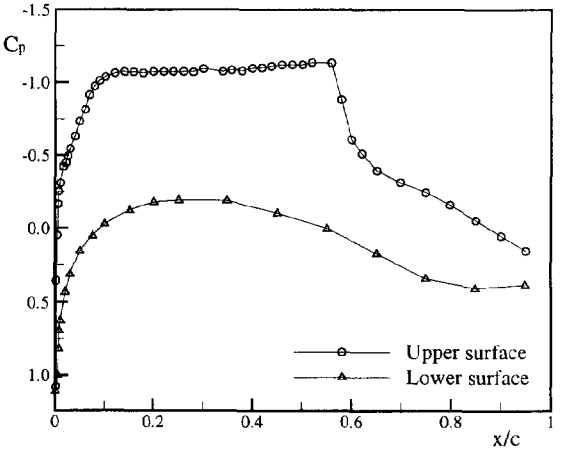

6f M=0.773, α=2.59°

Fig. 6 Steady pressure distributions

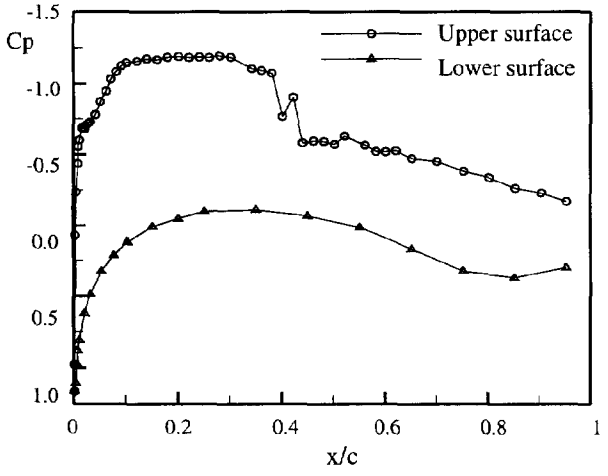

6g M=0.804, α=3.54°

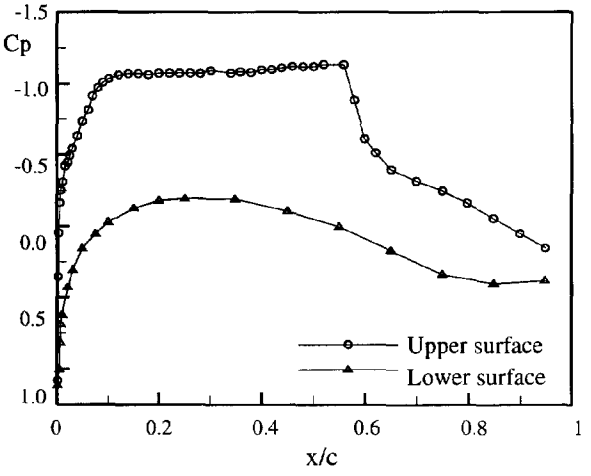

6h M=0.804, α=0.33°

Fig. 6(cont.) Steady pressure distributions

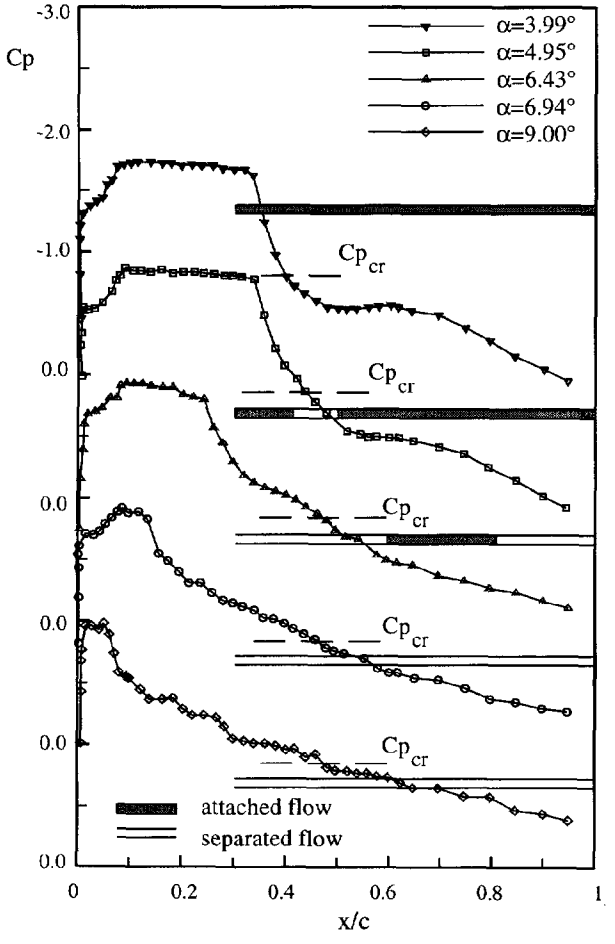

Fig. 7 Steady pressure distributions on upper surface at M=0.688

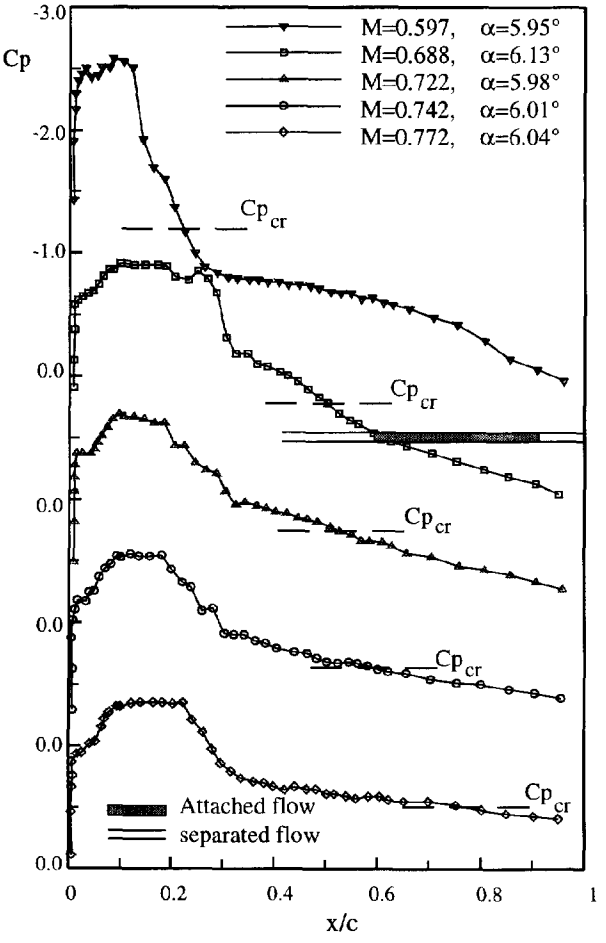

Fig. 8 Steady pressure distributions on upper surface at various Much numbers

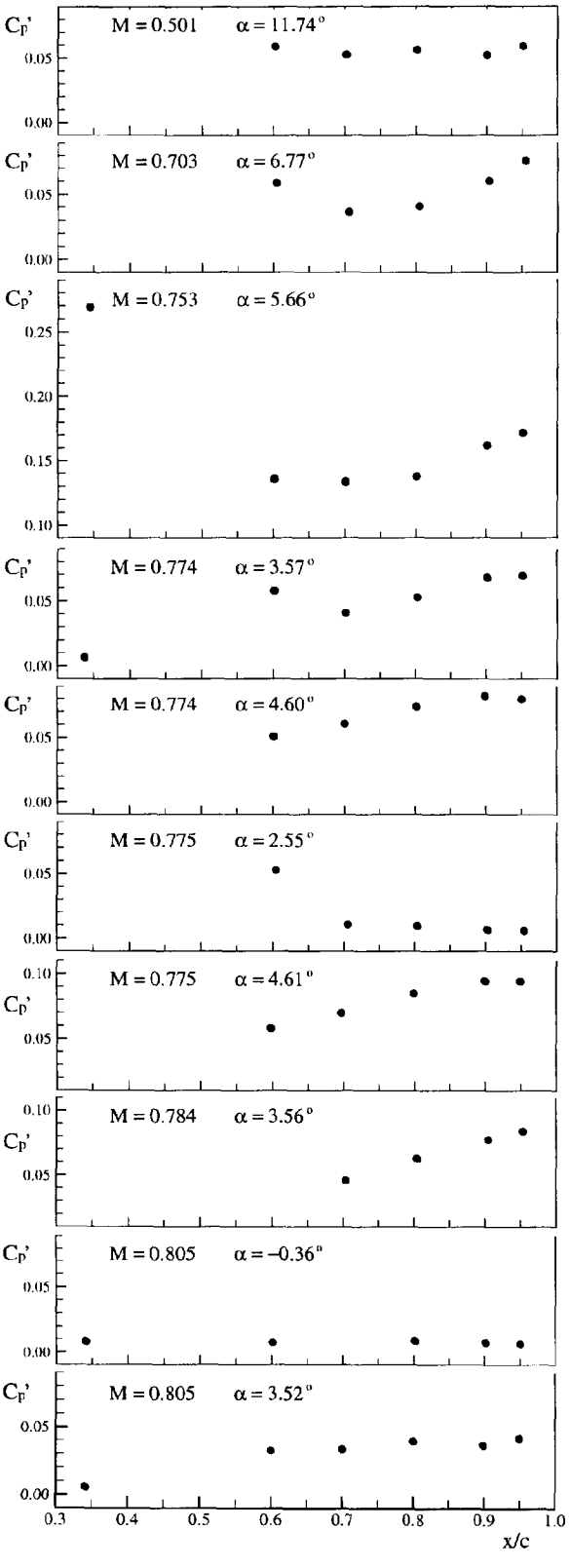

Fig.10 Variation of pressure intensities along airfoil chord

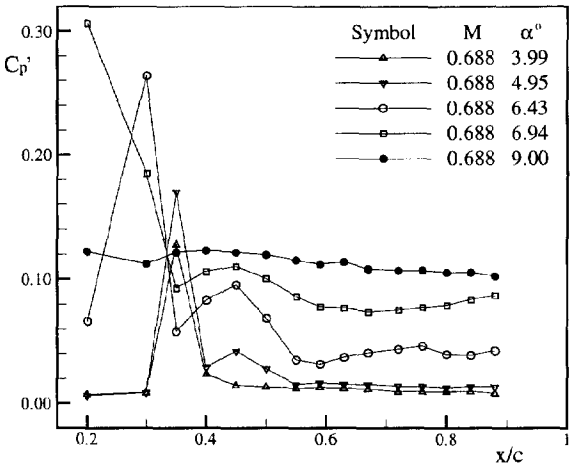

11a for points A,B,C,D and E in Fig.5

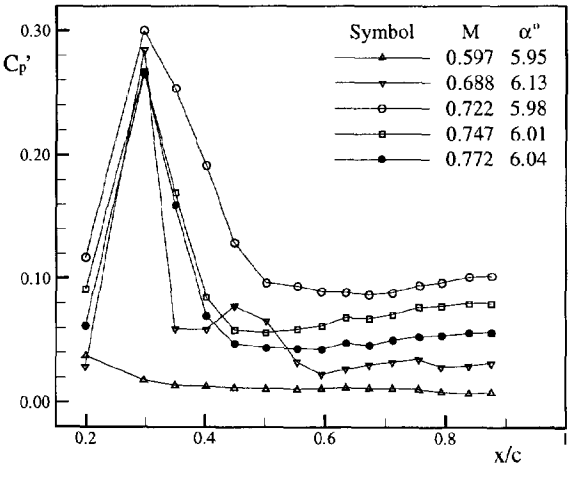

11b for points a,b,c,d and e in Fig.5

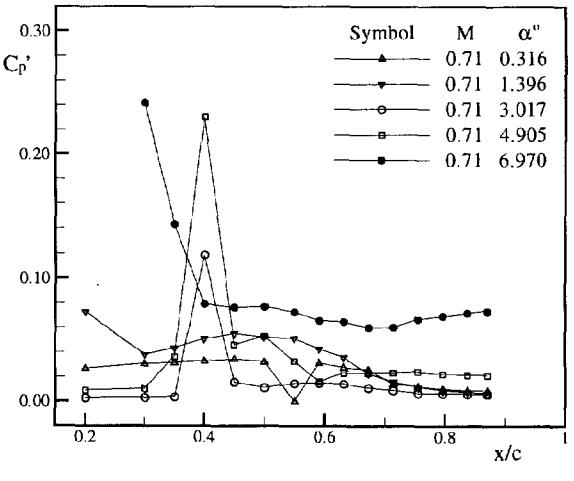

11c for points 1,2,3,4 and 5 in Fig.5

Fig.11 Unsteady pressure distributions

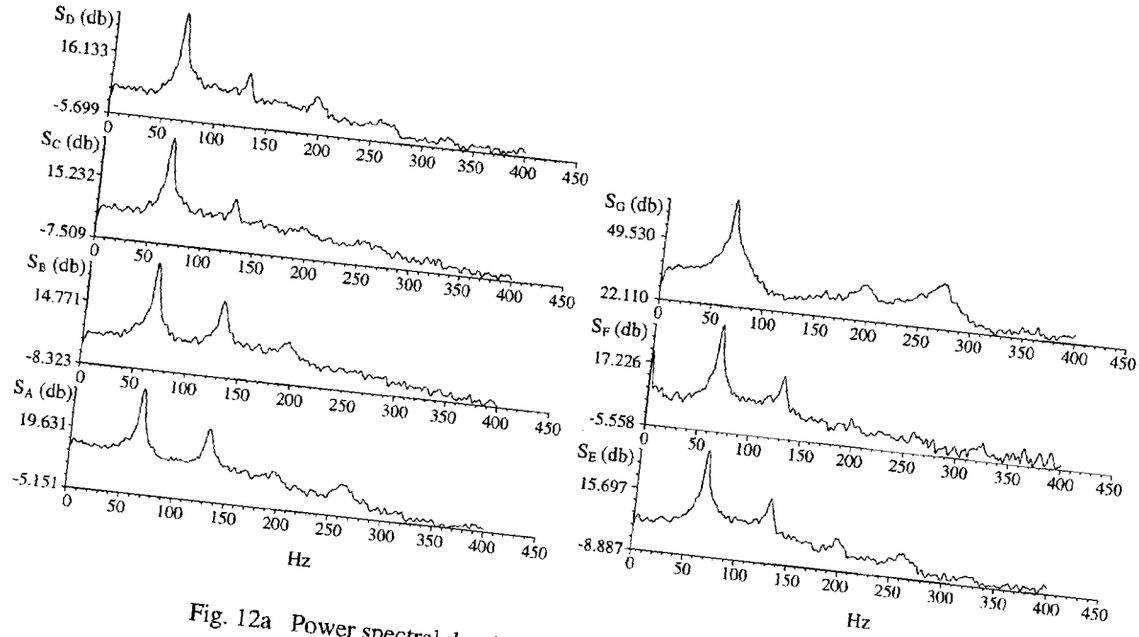

Fig. 12a Power spectral density for M_∞=0.753, C_L=0.945, q=24.5 psi

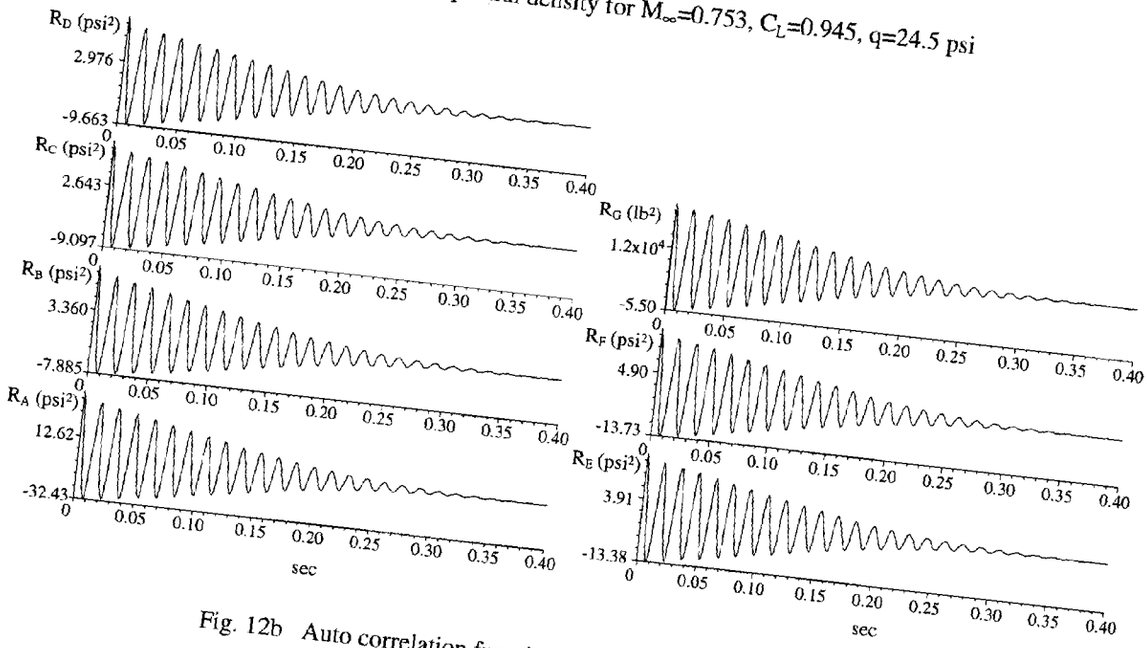

Fig. 12b Auto correlation functions for M_∞=0.753, C_L=0.945, q=24.5 psi

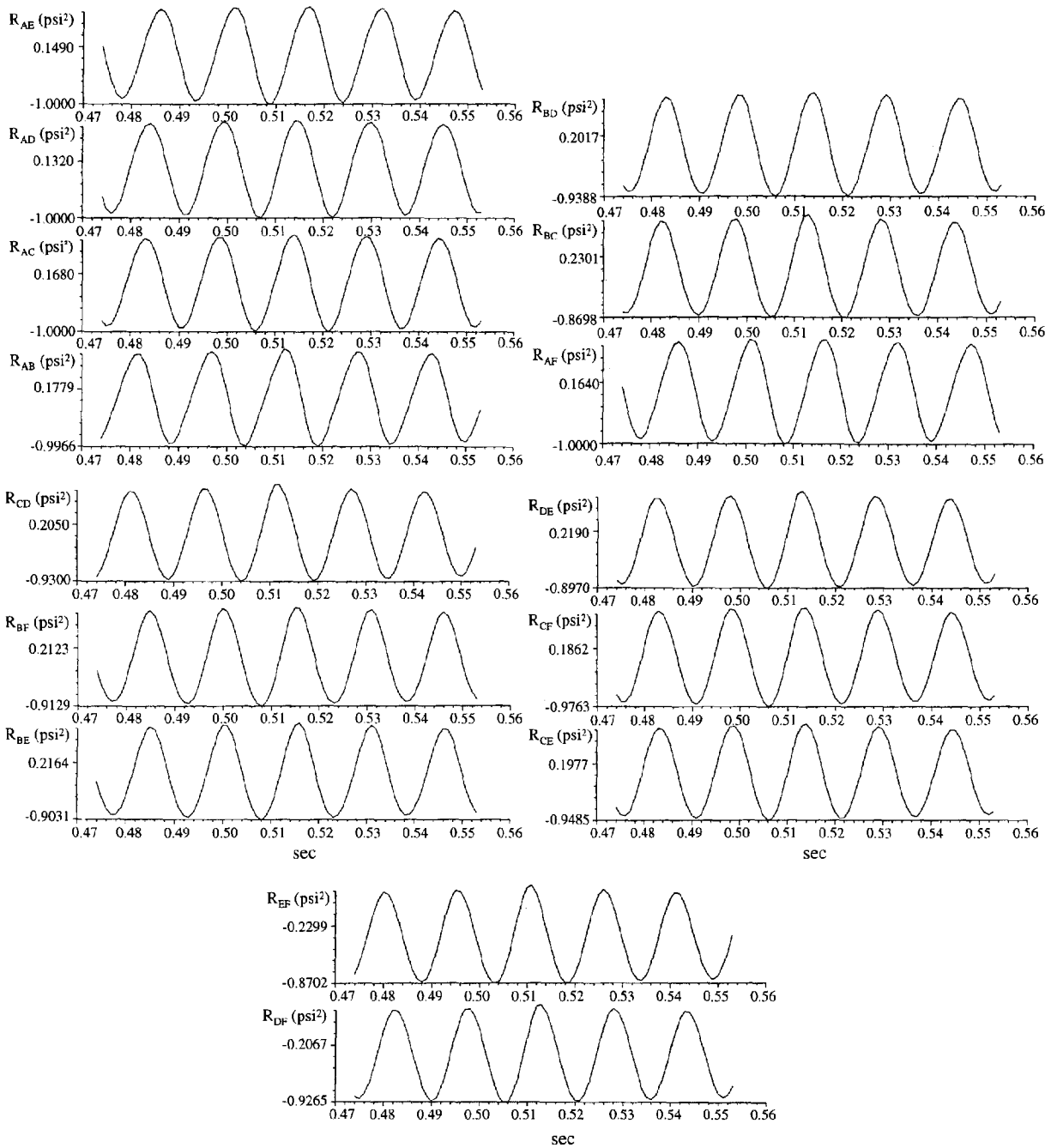

Fig. 12c Cross correlation functions for M_∞=0.753, C_L=0.945, q=24.5 psi

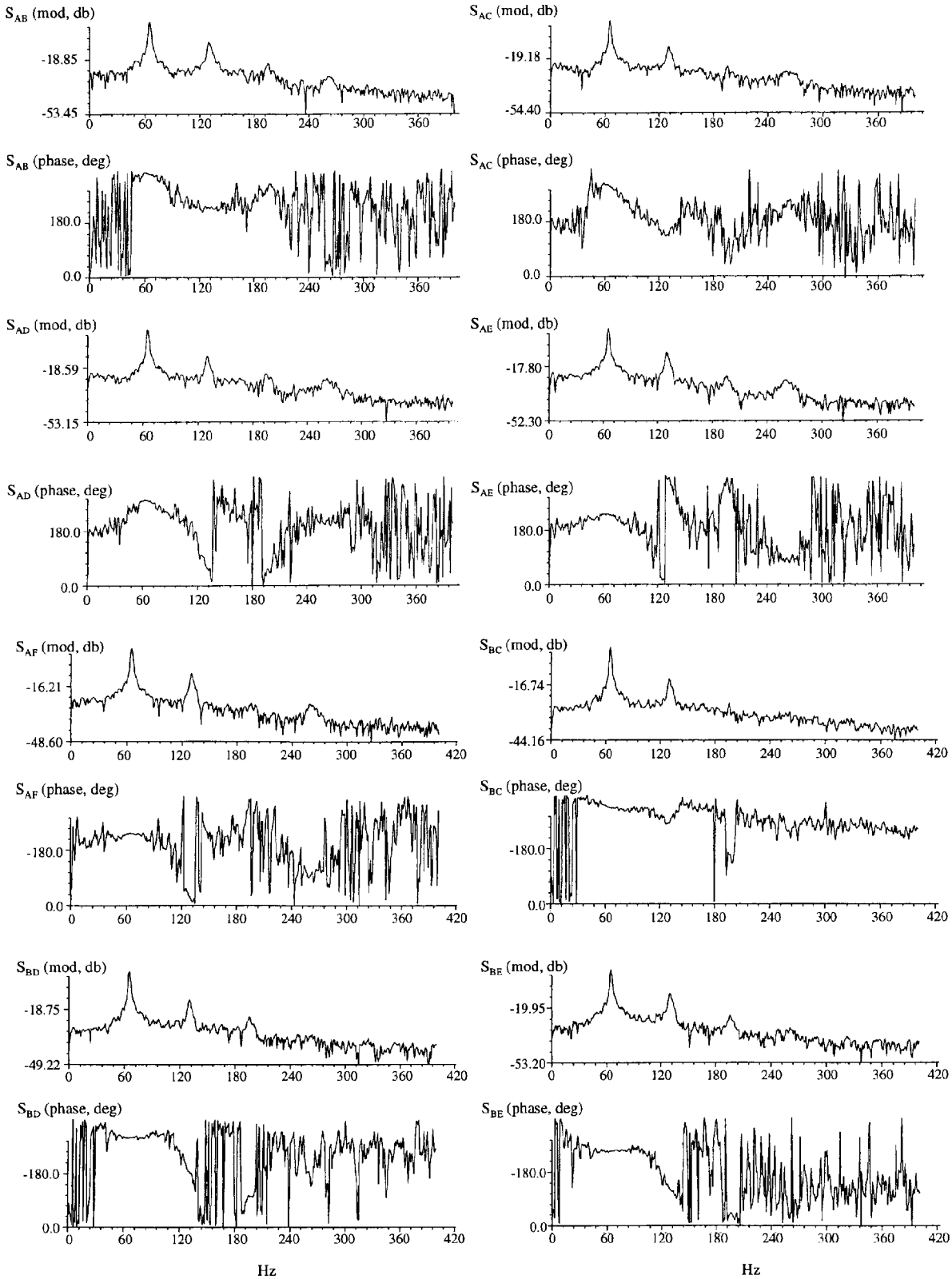

Fig. 12d Cross power spectral density for M_∞=0.753, C_L=0.945, q=24.5 psi

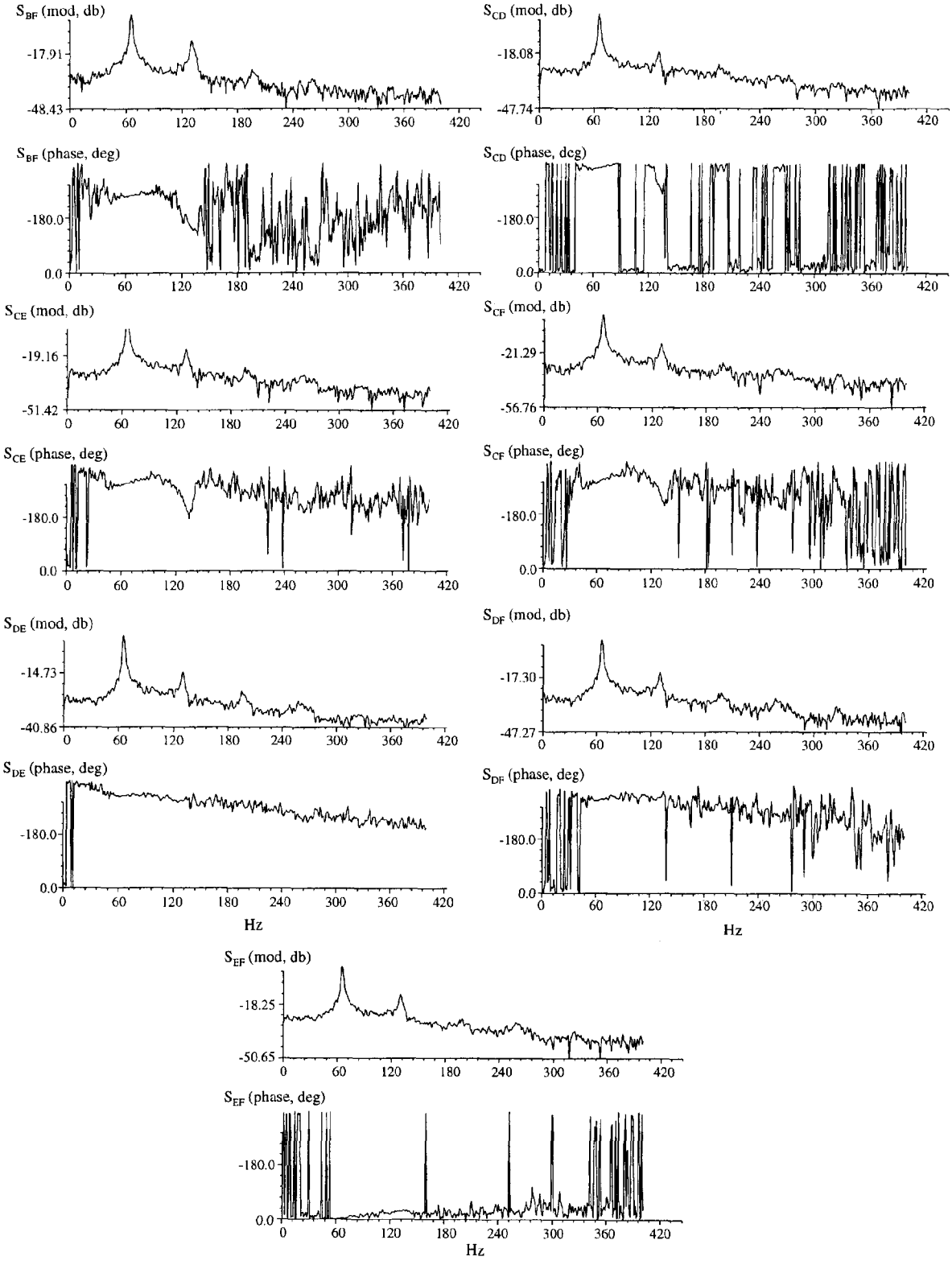

Fig. 12d (cont.) Cross power spectral density for M_∞=0.753, C_L=0.945, q=24.5 psi

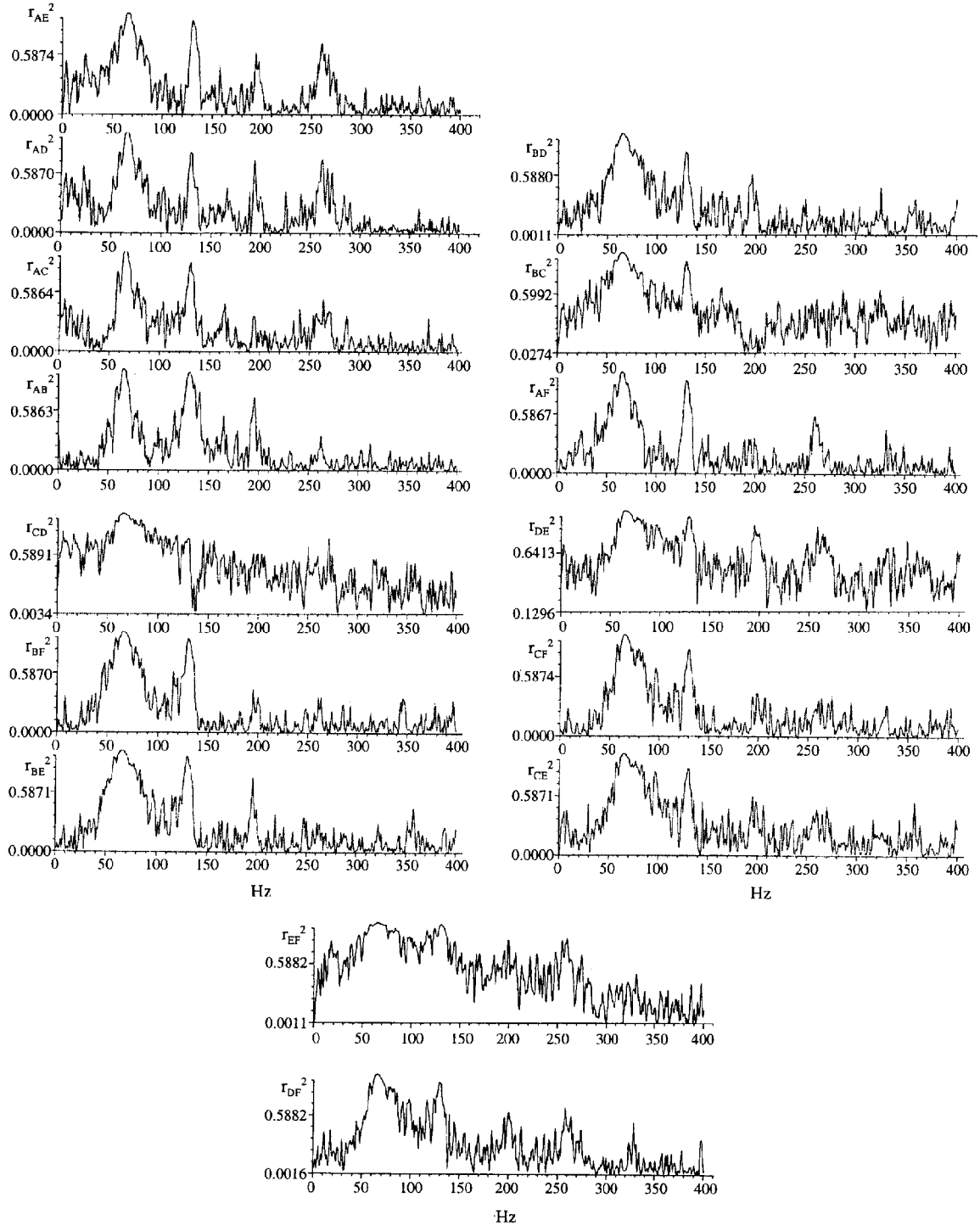

Fig. 12e Coherence functions for M_∞=0.753, C_L=0.945, q=24.5 psi

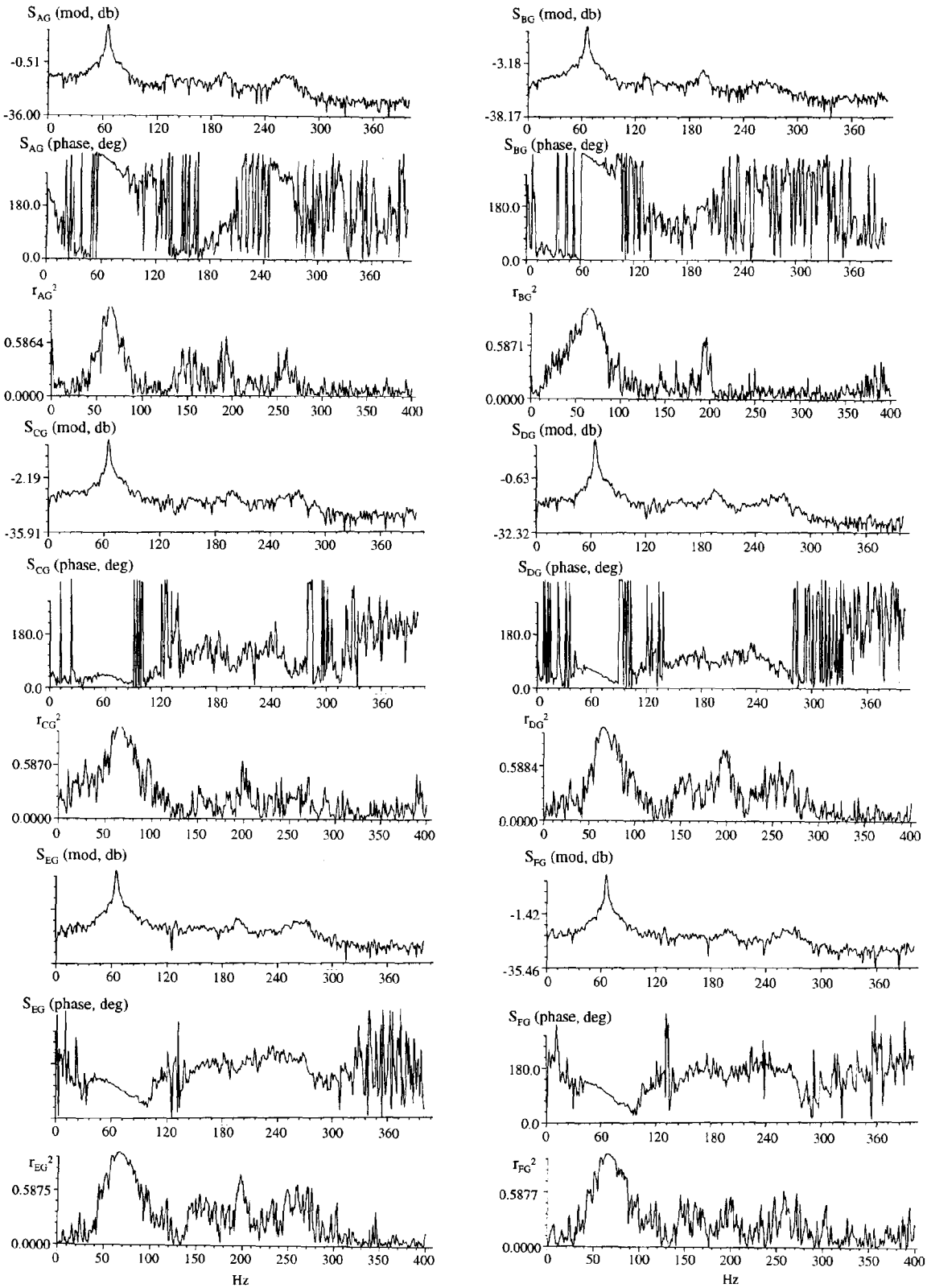

Fig. 12f Cross power spectral density and coherence function between pressure and normal force for M_∞=0.753, C_L=0.945, q=24.5 psi

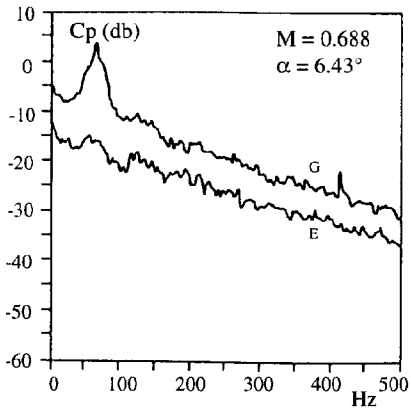

13a transducers located before and after shock

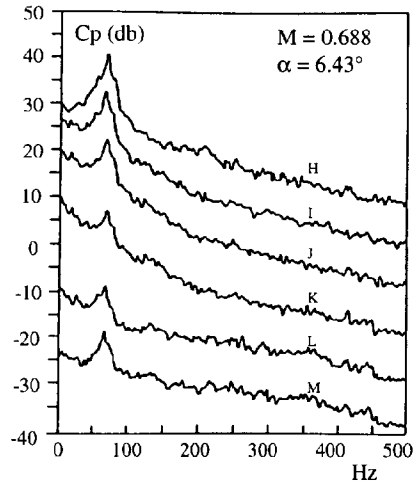

13b transducers located in the separation bubble

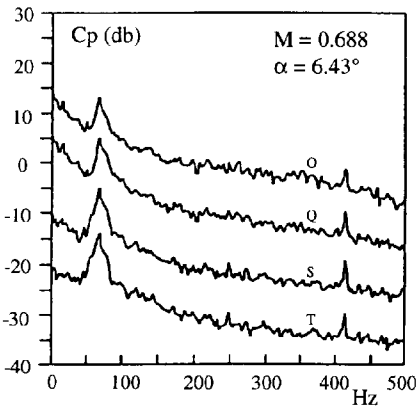

13c transducers located in the attachment and trailing-edge separation regions

Fig. 13 Power spectra of pressure on upper surface

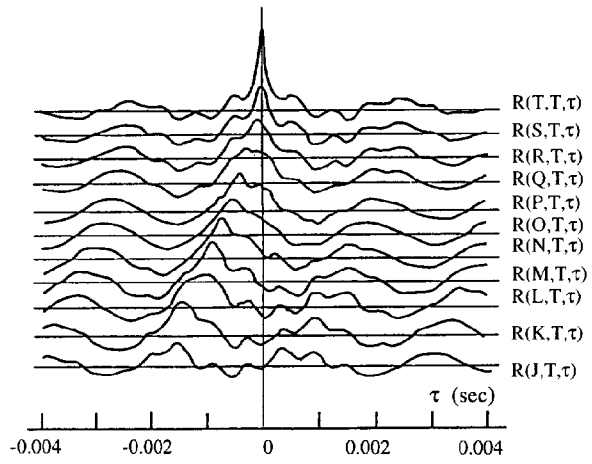

14a M = 0.688, α = 3.99°

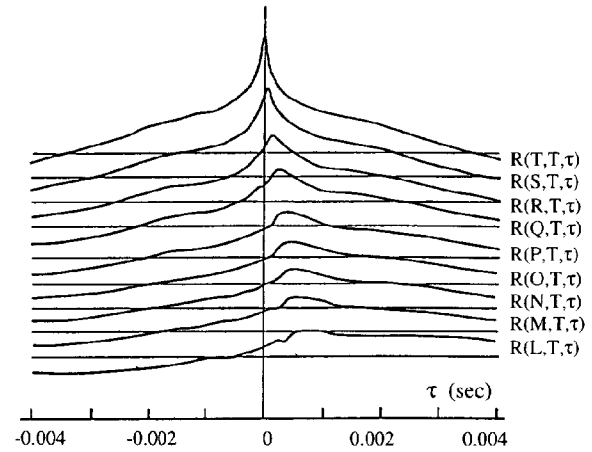

14b M = 0.688, α = 6.43°

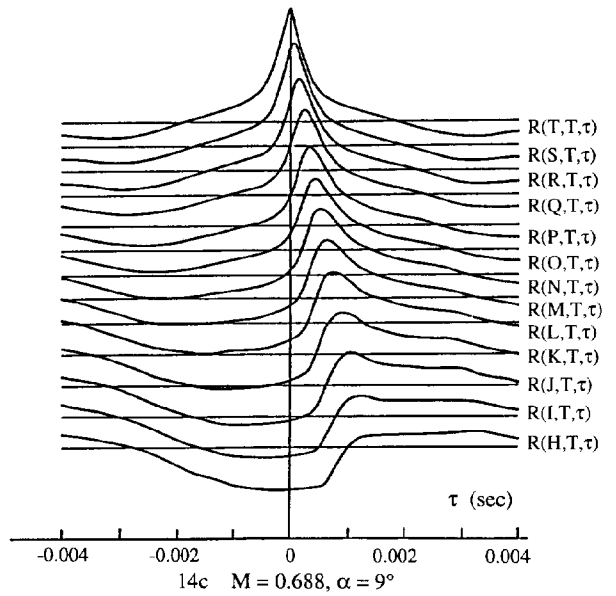

14c M = 0.688, α = 9°

Fig. 14 Cross-correlation functions of pressure

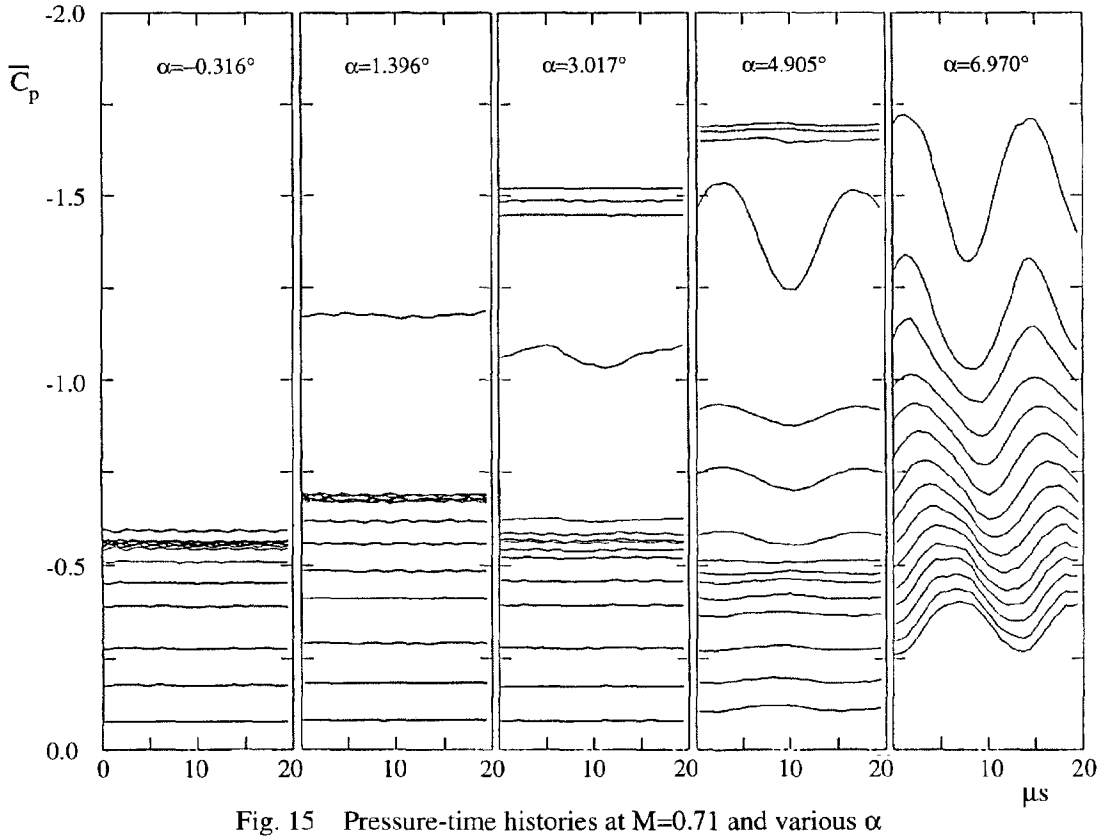

Fig. 15 Pressure-time histories at M=0.71 and various α

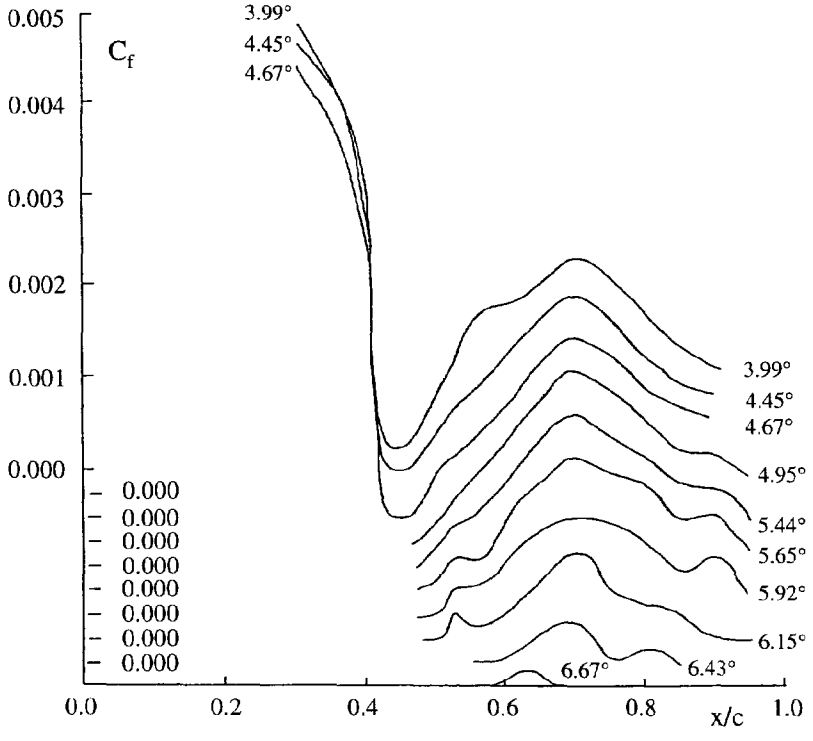

Fig. 16 Skin friction coefficient at M=0.688 and various α